

RSC Advances



This is an *Accepted Manuscript*, which has been through the Royal Society of Chemistry peer review process and has been accepted for publication.

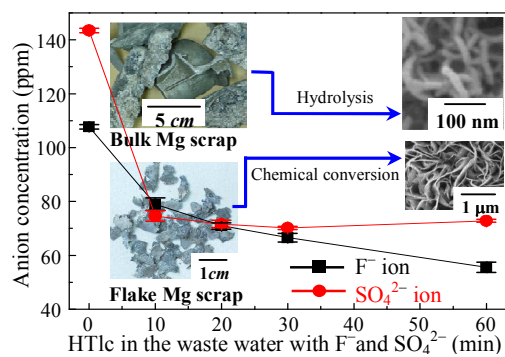
Accepted Manuscripts are published online shortly after acceptance, before technical editing, formatting and proof reading. Using this free service, authors can make their results available to the community, in citable form, before we publish the edited article. This *Accepted Manuscript* will be replaced by the edited, formatted and paginated article as soon as this is available.

You can find more information about *Accepted Manuscripts* in the [Information for Authors](#).

Please note that technical editing may introduce minor changes to the text and/or graphics, which may alter content. The journal's standard [Terms & Conditions](#) and the [Ethical guidelines](#) still apply. In no event shall the Royal Society of Chemistry be held responsible for any errors or omissions in this *Accepted Manuscript* or any consequences arising from the use of any information it contains.

Graphic Entry

This study converts waste magnesium scraps into nanomaterials which can function in use to simultaneously remove F^-/SO_4^{2-} in waste water.



Converting waste magnesium scrap into anion-sorptionable nanomaterials: synthesis and characterization of Mg–Al–Cl hydrotalcite-like compound by hydrolysis and chemical conversion treatment in aqueous chloride solutions

Yung-Feng Lung^a, Yu-Fan Syu^a, Meng-Chang Lin^b and Jun-Yen Uan^{a*}

^a *Department of Materials Science and Engineering, National Chung Hsing University, 250 kuo kuang Rd., Taichung 402, Taiwan, ROC*

^b *Green Energy and Environment Research Laboratories, Industrial Technology Research Institute, 195 Sec. 4, Chung-Hsing Road, Hsin-Chu 31040, Taiwan, ROC*

* *To whom correspondence and reprint requests should be addressed.*

Email: jyuan@dragon.nchu.edu.tw

Tel.: +886-4-22854913

Fax: +886-4-22857017

ABSTRACT

Although there have been many reports on the synthesis of hydrotalcite-like compound (HTlc), none of them have investigated the special case of converting metal waste into anion-sorptionable HTlc. Mg–Al alloy is the most commonly used Mg alloy. Most metallic Mg wastes and the post–consumer Mg products are, however, currently not recyclable, thus leaving the resources wasted. Here, methods that allow the reuse and recycling of the Mg wastes are demonstrated, employing a combination of hydrolysis and chemical conversion treatment in chloride acidic solutions that corrode the metallic wastes to develop Mg–Al–Cl HTlc. The study can convert bulk–type magnesium waste into nanosized Mg–Al–Cl HTlc powder. For fine flake–type magnesium waste, Mg–Al–Cl HTlc film can directly form on the surface of the flake. All the synthesized HTlcs have nanosized microstructures, being able to function in use to uptake most of the fluoride and sulfate anions from waste water.

Keywords: Nanomaterials; Anion sorption; Alloy; Waste recycling; Hydrotalcite like compound (HTlc); Magnesium waste scrap

1. Introduction

Material recycling is important to making products more environmentally sustainable over their life cycles.¹ In the automotive industry, the ability to recycle a material is regarded as an important aspect of its value.² Mg alloys and Al alloys are very attractive materials for use in lightweight vehicles.^{3, 4} A range of automotive components are made of Al and Mg alloys, including wheels, seat frames, and others.⁴ When cars and trucks that contain such materials reach the end of life, the scrap aluminum and magnesium can be recovered from the end-of-life vehicles. Scrap Al and Mg from end-of-life vehicles can be further separated from each other, but for economic reasons, Mg scrap ends up in the light metal fraction together with Al scrap, and is typically reused as an additive in aluminum alloys.² According to Mendis and Singh,⁵ given the increased use of Mg, a commercially viable method for separating Mg from Al is essential. Various studies^{2, 3, 6-8} have investigated new methods for the metallurgical recycling of scrap Mg in all instances from end-of-life products. For example, according to Javaid *et al.*,⁷ when Mg alloys are mixed or contain impurity elements, they cannot easily be recycled. Fechner *et al.*⁶ and Blawert *et al.*⁸ tried to develop a secondary magnesium alloy system with improved tolerance of impurities for the new alloy system coming from mixed magnesium post-consumer scrap. Currently, low-grade magnesium scraps and post-consumer Mg alloys (e.g., coated (Cu, Ni) magnesium) are not recycled.⁹ Most magnesium products are manufactured by the die casting process,¹⁰ which generates Mg flash scrap.¹¹ Flash scrap (as will be presented in Fig. 3) is thinner than other Mg scraps at about 0.3 mm thick. Since oxide and slag are easily formed when fine flash scrap is dumped into a melting furnace, the flash scrap cannot be recycled into secondary Mg ingots. In fact, according to Javaid *et al.*,⁷ Mg scraps that contain oxide particles cannot easily be recycled, potentially resulting in the Mg resource wasted. In 2009, the authors of the present study developed a method for reusing Mg scraps in a hydrogen generator.¹² Recently, Ehrenberger

and Friedrich² suggested that owing to its potential to reduce CO₂ emissions from the production of primary magnesium, the reuse of Mg alloy scraps is a promising means of improving the environmental performance of Mg alloys.

HTlc is a well-known layered material with a general formula $[M^{2+}_{1-x}M^{3+}_x(OH)_2]^{x+}(A^{n-}_{x/n}) \cdot nH_2O$.¹³ M^{2+} and M^{3+} denote divalent and trivalent metal cations, respectively, such as Mg^{2+} and Al^{3+} . A^{n-} is an anion, such as CO_3^{2-} , F^- or Cl^- . The affinities of various anions toward the interlayer spaces of HTlcs follow the order, $CO_3^{2-} > SO_4^{2-} > OH^- > F^- > Cl^- > Br^- > NO_3^- > I^-$.¹⁴ Therefore, of Mg–Al– A^{n-} HTlc, where A^{n-} is CO_3^{2-} , SO_4^{2-} , F^- or Cl^- , Mg–Al–Cl HTlc exhibits greater anion exchangeability than Mg–Al– A^{n-} HTlc ($A^{n-} = CO_3^{2-}$, SO_4^{2-} , F^-). Coprecipitation,¹⁵ sol-gel process¹⁶ and ammonia release^{17, 18} are traditional methods for synthesizing HTlc powders. Some new methods have also been recently reported.¹⁹⁻²¹ HTlc powders are utilized for catalysis,²² adsorbents,²³ drug storage²⁴ or CO₂ capture.^{25, 26} For example, Choudary *et al.*^{22, 27, 28} utilized Mg–Al–Cl HTlc powders to perform catalytic reactions. A typical method for synthesizing Mg–Al–Cl HTlc powder is coprecipitation in mixed solutions of $MgCl_2$ and $AlCl_3$ at pH 10.²⁹ Another method for producing Mg–Al–Cl HTlc powder involves the deintercalation of carbonate ions from the interlayer of HTlcs.^{17, 30} Costantino *et al.*¹⁷ generated Mg–Al–Cl HTlc by passing gaseous HCl through Mg–Al–CO₃ HTlc at 150 °C for 8 h. In the range 140–160 °C, carbonate ions in the interlayer are deintercalated and be replaced by chloride ions.¹⁷ Iyi *et al.*³⁰ deintercalated carbonate ions by immersing Mg–Al–CO₃ HTlc powder in various concentrations of HCl solutions for 24 h. The carbonate content in Mg–Al–CO₃ HTlc was effectively reduced to almost zero by immersing the HTlc powder in highly concentrated HCl solutions (0.03 N). However, the weight loss was approximately 50% of the original weight of input of the HTlc powder. Iyi *et al.*³⁰ made great progress in developing a mixed solution of dilute HCl (0.005 N)

and highly concentrated NaCl (25 wt.%) to conduct the deintercalation of the carbonate ions in Mg-Al-CO₃ HTlc. Around 60 % of the carbonate in the Mg-Al-CO₃ HTlc was deintercalated by immersing the Mg-Al-CO₃ HTlc powder in the 25 wt.% NaCl solutions for as long as 24 h. However, the use of highly concentrated NaCl solutions yielded a mixture of residual salt and the final HTlc products. Therefore, the product had to be washed several times in decarbonated and deionized water.³⁰ In the new method, developed in the present study, aqueous HCl with an initial pH of 1.5 (0.03N), containing only 3.5 wt.% NaCl, was used to develop an Mg-Al-Cl HTlc film directly on the surface of Mg alloy flash scrap in a single step. The low concentration, 3.5 wt.%, of the NaCl solution (c.f., 25 wt.%³⁰) should reduce the amount of residual salt that mixed with the final Mg-Al-Cl HTlc product, eliminating the need for washing several times using water.

In 2007, the authors of this paper developed a novel method for producing an Mg-Al-CO₃ HTlc film on Mg-Al alloy to protect it against corrosion.^{31,32} Lin *et al.*³³, Chen *et al.*³⁴ and Zhang *et al.*³⁵ investigated the mechanism of growth of the Mg-Al-CO₃ HTlc film on Mg-Al alloy. Recently, Ishizaki *et al.*³⁶ made great process in improving the corrosion resistance that is provided by the Mg-Al-CO₃ HTlc film on Mg alloy. However, since the affinities of various anions toward interlayers of HTlcs follow the order CO₃²⁻ > SO₄²⁻ > OH⁻ > F⁻ > Cl⁻ > Br⁻ > NO₃⁻ > I⁻,¹⁴ carbonate ions exhibit the highest affinity to the interlayers of HTlcs. To extend the range of possible applications of the HTlc obtained from Mg scraps, this study focuses on the formation of Mg-Al-Cl HTlc powder and its thin film. To the best of the authors' knowledge, this study is the first to examine whether Mg alloy scraps can be applied to the formation of Mg-Al-Cl HTlc powder. No investigation has before been published on the direct growth of Mg-Al-Cl HTlc film on Mg-Al alloy substrate.

Briefly, this work will establish a possible means of reusing low-grade Mg scraps. According to previous study,³⁷ $\text{Al}_{12}\text{Mg}_{17}$ intermetallic compound was prepared by melting pure magnesium and pure aluminum in an induction furnace under vacuum. For application, the $\text{Al}_{12}\text{Mg}_{17}$ could absorb hydrogen at temperature over 200 °C and desorb hydrogen at 340 °C.³⁷ Here, we successfully prepare $\text{Al}_{12}\text{Mg}_{17}$ by melting bulk magnesium scrap and aluminum scrap in a furnace in air. This study develops novel processes to convert the $\text{Al}_{12}\text{Mg}_{17}$ into Mg–Al–Cl HTlc nanomaterial. Additionally, a new aqueous solution (pH 1.5 HCl aqueous with 3.5 wt.% NaCl) that can easily be used to form a conversion coating (Mg–Al–Cl HTlc thin film) on the surfaces of Mg flake scraps is developed. The performance of the HTlc in taking up fluoride and/or sulfide anions from waste water is evaluated. Anion intercalation within interlayer spaces in HTlc was not the dominant mechanism of removal of most F^- from the solution. Residual positive charge (RPC) was measured, and found to be useful for evaluating the F-uptake ability of an HTlc compound.

2. Experimental

2.1 Preparing $\text{Al}_{12}\text{Mg}_{17}$ powder for producing Mg–Al–Cl HTlc powder

To convert bulk-type waste metal scraps into anion-exchangeable Mg–Al–Cl HTlc powder at a relatively high rate, the scrap metal bulk must be powdered first. Since Mg alloy waste (as displayed in Fig. 1(a)) and pure Al wire cable scrap (Fig. 1(b)) are both ductile materials, neither of which can be efficiently ground by hand into powder. According to previous work,³⁷ $\text{Al}_{12}\text{Mg}_{17}$ intermetallic compound (containing 42 wt.% Al and 58 wt.% Mg) is weak and brittle. The compound can be pulverized easily, followed by being ground into powder. In this study, Mg–Al alloy scrap (Fig. 1(a)) and Al cable wire scrap (Fig. 1(b)) are utilized as the raw materials in the preparation of $\text{Al}_{12}\text{Mg}_{17}$ IMC. The raw materials were

melted together in a graphite crucible, and the molten metal was poured (at 600 °C) into a metal mold to solidify. Figure 1(c) presents the as-cast $\text{Al}_{12}\text{Mg}_{17}$ IMC ingot thus formed. Figure 1(d) displays the X-ray pattern of the as-cast ingot, which includes X-ray peaks of $\text{Al}_{12}\text{Mg}_{17}$ only (JCPDS card 1-1128). The material was not pyrophoric and could be safely handled in air. The as-cast $\text{Al}_{12}\text{Mg}_{17}$ sample was crushed by hand into small pieces (Fig. 2(a)) and ground by hand to a powder in a mortar (Fig. 2(b)). A 0.625 g mass of the $\text{Al}_{12}\text{Mg}_{17}$ powder was immersed in 250 mL of deionized water at 60 °C. Mixing was followed by the continuous addition of aqueous HCl to the mixture. Ar gas (at a flow rate of 0.5 LPM) was bubbled through the solution to reduce contamination by CO_2 . The pH value was maintained at approximately pH 1 by adding aqueous HCl acid dropwise with vigorous stirring. The $\text{Al}_{12}\text{Mg}_{17}$ powder was hydrolyzed in the acidic solution in around 30 min. The concentration of cations in the solution was determined by inductively coupled plasma atomic emission spectroscopy (ICP-AES) (ULTIMA 2000, Horiba Jobin Yvon). When 0.625 g of $\text{Al}_{12}\text{Mg}_{17}$ was dissolved in aqueous acid (250 mL), the aqueous solution contained approximately 1402 ppm Mg^{2+} and 1098 ppm Al^{3+} . The solution then contained the necessary anion (Cl^-) and cations (Mg^{2+} and Al^{3+}) for the subsequent synthesis of Mg-Al-Cl HTlc powder. This solution was cooled to room temperature. Aqueous NaOH (2.5 M) was added dropwise to the solution with vigorous stirring until the pH of the solution reached the desired value (pH 8, 9, 10, or 11), which was maintained for 10 min. The simultaneous stirring and bubbling of Ar were not interrupted during this synthetic process. A white precipitate formed as a suspension in the solution. The suspension was filtered using a centrifuge, and washed with deionized water. All of the precipitates were then immediately dried in a vacuum. HTlc-Cl_pH11 denotes the HTlc powder that was fabricated by dissolving $\text{Al}_{12}\text{Mg}_{17}$ powder in $\text{HCl}_{(\text{aq})}$ and then adding $\text{NaOH}_{(\text{aq})}$ dropwise to increase the pH of the solution from pH 1 to pH 11, which was maintained for 10 min. Similarly, HTlc-Cl_pH8 was formed by adding $\text{NaOH}_{(\text{aq})}$ to increase the pH of the

solution from pH 1 to pH 8, which was maintained for 10 min.

The crystallographic structures of the synthetic products were identified by X-ray powder diffraction using a Bruker D2 Phaser diffractometer with Ni-filtered Cu $K\alpha_1$ (1.5406 Å) radiation. The synthetic products also underwent Fourier transform infrared (FT-IR) analysis using a Perkin-Elmer Spectrum RX-I spectrometer. For FT-IR, each powdered sample was mixed with oven-dried spectroscopic-grade KBr. The mixture was then pressed into a disc with a diameter of 12.91 mm under around 8 tons of pressure for one minute in a vacuum. FT-IR spectra were obtained at wavenumbers from 400 to 4000 cm^{-1} . Elemental chemical analyses of the synthetic products were carried out by energy dispersive spectrometry (EDS) using an Oxford INCA Energy-350 microanalysis system and an INCA Wave-500 that was attached to a JEOL JSM-7000F field emission scanning electron microscope.

Industrial waste water (100 mL), comprising about 200 ppm F^- and 200 ppm SO_4^{2-} , was used to evaluate the ability of the synthesized powder to uptake fluoride and sulfide ions from waste water. In the experiment, the solution was purged with argon to reduce the effect of carbonate anions formed from the atmospheric gaseous CO_2 . In the experiments, 0.35 g and 0.7 g of Mg–Al–Cl HTlc_pH10 were used. Dilute nitric acid (2 vol.%) was used to maintain the pH of the solution at 6.0 ± 0.5 throughout the absorption experiment). Concentrations of residual F^- and SO_4^{2-} in the industrial waste water were simultaneously measured using ion chromatography (IC) (ICS-900, Dionex). The errors in the F^- and SO_4^{2-} concentrations that were caused by adding nitric acid to maintain the solution pH at 6.0 ± 0.5 were under 5%.

2.2 Flake (flash) scraps and aqueous solutions for forming Mg–Al–Cl HTlc thin film thereon

Flash scraps from AM60 and AZ91 die casting (Figs. 3 (a) and (b)) were used in this study. AM60 contained 6.0 wt.% Al and 0.13 wt.% Mn; AZ91 comprised 9.0 wt.% Al and 0.7

wt.% Zn. Flash scraps were smashed into small pieces (around $0.3 \times 3 \times 3 \text{ mm}^3$, as shown in the bottom of Fig. 3 (c)), and then deoiled. An aqueous solution of 3.5 wt.% NaCl at pH 1.5 (reached by the dropwise addition of 10.4 M HCl) was prepared. This aqueous solution, denoted as NaCl_pH 1.5, was used to develop conversion coating (Mg–Al–Cl HTlc) on AM60 and AZ91 Mg flash scraps.

AM60 contains 6 wt.% Al, which is approximately 3 wt.% less than the weight percentage in AZ91 alloy. Owing to the low Al concentration, a unique solution was prepared for coating AM60 flash scrap by dissolving AlCl_3 in NaCl_pH 1.5 aqueous. The solution with 0.02 g AlCl_3 added to 200 ml NaCl_pH 1.5 aqueous is denoted as $\text{AlCl}_3^{0.02}$ _NaCl_pH 1.5. Similarly, $\text{AlCl}_3^{0.22}$ _NaCl_pH 1.5 is the solution formed by adding 0.22 g AlCl_3 to 200 ml NaCl_pH 1.5 aqueous. Argon gas was bubbled through each solution throughout the conversion treatment to reduce contamination by carbonate.

2.2.1 Formation of Mg-Al-Cl HTlc film on surface of flash scrap. A 1.5g mass of flash scrap was added to NaCl_pH 1.5 solution (200 ml) with stirring at room temperature. Argon gas was bubbled through the solution to reduce contamination by carbonate during the chemical conversion surface treatment. The AM60 and AZ91 scrap samples that had been treated in NaCl_pH 1.5 aqueous for 30 min were denoted as AM60_HTlc^{30min} and AZ91_HTlc^{30min}, respectively. AM60 flash scrap (1.5 g) was separately treated in NaCl_pH 1.5, AlCl₃^{0.02}_NaCl_pH 1.5 and AlCl₃^{0.22}_NaCl_pH 1.5 aqueous solutions, for 30 min at room temperature. The reaction time 30 min was selected because the solution pH would reach to a static value after 30 min reaction in the NaCl_pH 1.5 aqueous. The post-treated AM60 samples (treated in the AlCl₃-added aqueous) were denoted as AM60^{0.02}_HTlc^{30min} and AM60^{0.22}_HTlc^{30min}. In the notation, the first superscript indicates the amount of AlCl₃ that was added to 200 ml of NaCl_pH 1.5 solution, and the second superscript indicates the duration of the treatment.

Crystallographic data were obtained from each coated material by glancing angle X-ray diffraction (GAXRD) using a glancing angle of 0.5° under Cu K_{α1} (1.5406 Å) radiation. Microstructures were studied using a field-emission scanning electron microscope (SEM, JEOL JSM - 6700F), which was equipped with an energy dispersive spectrometer (EDS) connected to an Oxford Inca Energy-350 microanalysis system. Following the work of Ishizaki *et al.*³⁶ on SEM-EDS analysis, herein, the compositions of the Mg-Al-Cl HTlc films on the Mg flake scraps were determined by SEM-EDS area scanning (30×30 μm²) at 10 keV. A Fourier transform infrared (FT-IR) spectrum of the Mg-Al-Cl HTlc was obtained using a DIGILAB FTX3500 instrument at wavenumbers from 400 to 4000 cm⁻¹. The Mg-Al-Cl HTlc powder (0.001 g) for FT-IR analysis was taken from the surface of an HTlc-coated scrap by lightly scraping its surface with a surgical blade. The powder thus obtained was combined with oven-dried spectroscopic-grade KBr (0.1 g). The mixture of the HTlc powder and the

KBr was pressed into a disc (with a diameter of 12.91 mm) under eight tons of pressure for 1 min in a vacuum before the FT-IR measurements were made.

2.2.2 Removal of fluoride ions from fluoride-containing water by the HTlc-coated scraps.

An aqueous (100 ml) solution of 100 ppm fluoride ion was prepared using NaF standard solution (Merck). HTlc-coated flake scrap with a total mass of 1.5 g was immersed in the F^- -containing solution (pH 6.0 ± 0.5) with stirring. Ion chromatography (IC; ICS-900, DIONEX) was used to measure the residual fluoride concentration at 10 min, 20 min, 30 min and 60 min. The errors in the fluoride concentration that were caused by adding nitric acid to maintain the pH of the solution at 6.0 ± 0.5 were less than 5 %.

3. Results and Discussion

3.1 Converting bulk Mg scrap into HTlc powder

3.1.1 Formation of Mg-Al-Cl HTlc powder from acidic to alkaline environment.

Figure 4(a) presents the X-ray powder diffraction patterns of the synthesized Mg-Al-Cl HTlc powder. The bottom of Fig. 4(a) shows, in order, the patterns of HTlc-Cl_pH8, HTlc-Cl_pH9, HTlc-Cl_pH10, and HTlc-Cl_pH11. Gibbsite and brucite peaks were detectable following treatment at pH 8 or pH 9 at room temperature. The peaks were absent following treatment at pH 10 or pH 11 (See the X-ray patterns of HTlc-Cl_pH10 and HTlc-Cl_pH11 in Fig. 4(a)). The X-ray peaks at 11.22° and 22.38° were identified as basal reflections of hydrotalcite. However, the XRD reflection peaks were shifted to lower 2-theta values than those of a typical Mg-Al- CO_3 HTlc (JCPDS 22-700, $[Mg_6Al_2(OH)_{16}](CO_3) \cdot 4(H_2O)$). The basal spacing is well known to vary with the size of the intercalated anions.¹⁴ The Mg-Al-Cl HTlc had a (003) basal spacing of 0.788 nm (Fig. 4(a)), which is similar to corresponding values for Mg-Al-Cl HTlc that have been obtained elsewhere,³⁸⁻⁴⁰ exceeds that of the

carbonate-intercalated hydrotalcite Mg-Al-CO₃ HTlc (0.769 nm),³⁸⁻⁴⁰ indicating that the carbonate ion was not the dominant anion in the HTlc. The results of the FT-IR analysis of the Mg-Al-Cl HTlc powder in Fig. 4(b) reveal an absorption band at 1372 cm⁻¹, whose intensity was determined by carbonate ions.³⁸⁻⁴⁰ However, the intensity of this band was much lower than the typical band intensity of carbonate ions in Mg-Al-CO₃ HTlc.⁴⁰ The substantial absorption that was observed at 3470 cm⁻¹ was attributed to the H-bonding stretching vibrations of the OH group ($\nu_{\text{O-H}}$) in the brucite-like layer.⁴¹ The presence of a band at 1640–1650 cm⁻¹ was attributed to the bending vibration ($\delta_{\text{H}_2\text{O}}$)⁴¹ of the H₂O molecules in the interlayers and the surface absorbent. The typical lattice vibration bands ($\nu_{\text{M-O}} = 678 \text{ cm}^{-1}$ and $\delta_{\text{M-O-H}} = 448 \text{ cm}^{-1}$)^{39, 42} of the brucite-like layers were identified at low wavenumbers. In the spectra of HTlc-Cl_pH8 and HTlc-Cl_pH9, the absorption band at 1028 cm⁻¹ is attributable to the hydroxyl bending vibration δ_{OH} ^{43, 44} in gibbsite. The hydroxyl bending vibration δ_{OH} that was observed in the FT-IR spectra was absent from the spectra of HTlc-Cl_pH10 and HTlc-Cl_pH11. This result is consistent with the X-ray diffraction patterns of HTlc-Cl_pH10 and HTlc-Cl_pH11 (Fig. 4(a)), which include no X-ray peak associated with gibbsite. However, neither X-ray diffraction nor FT-IR provided direct evidence of the presence of Cl⁻ in the HTlc. Figure 4(c) shows the EDS spectrum of HTlc-Cl_pH10, including a Cl peak but no detectable Na peak. Thus, the intensity of the Cl peak in Fig. 4(c) EDS spectrum did not arise from the NaCl(s) on surface of the sample. Rather, Cl⁻ ions were intercalated in HTlc during the synthetic process. The microstructure of HTlc-Cl_pH10 was as shown in Fig. 4(d), showing nanoplatelets in the HTlc-Cl_pH10. Strong evidence will be presented later (Fig. 6) that the removal of F⁻ and SO₄²⁻ from waste water involves the uptake of anions by the synthesized HTlc-Cl_pH10.

The hydrolysis of Al₁₂Mg₁₇ powder in an acidic aqueous solution converted the Al₁₂Mg₁₇

powder into Al^{3+} and Mg^{2+} . With respect to recycling, the major contribution of the method that is developed in this study is that no metal ions are left in the solution after the process. Figure 5(a) plots the residual concentrations of Al^{3+} and Mg^{2+} ions in an aqueous solution following the synthesis of Mg–Al–Cl HTlc powder: Al^{3+} ions were almost undetectable after the synthesis when the solution was maintained at pH 8, pH 9 or pH 10. The residual Al^{3+} concentration was slightly greater when HTlc was synthesized using a solution that was maintained at pH 11. The residual magnesium ions were almost undetectable when the pH of the solution that was used in the synthesis of the HTlc was maintained at a high value (Fig. 5(a)). All of the Mg^{2+} and Al^{3+} ions in the solution were consumed to form Mg–Al–Cl HTlc when the solution was maintained at pH 9.5 ~ 10. Figure 5(b) reveals that the mass of the synthetic products varied with the pH that was maintained. The mass of the synthesized Mg–Al–Cl HTlc powder increased with the pH up to around pH 10, which maximized the mass of the synthesized product. Therefore, the results shown in Figs. 5(a) and (b) are consistent with each other, revealing that when all of the cations were consumed under the experimental conditions that included a maintained pH of the solution of approximately pH 10 during the synthesis of the HTlc (Fig. 5(a)), the yield of the synthetic product was maximized (Fig. 5(b)).

3.1.2 HTlc-Cl_pH10 to be in use for removal of F^- and SO_4^{2-} from waste water. Figure 6 plots the capacity of the synthesized product to take up F^- from waste water. The original aqueous solution that was used in the tests contained both ~ 200 ppm of fluoride ions and ~ 200 ppm of sulfide ions. A 0.35 g mass of HTlc-Cl_pH10 was immersed in the solution, and the absorptions of fluoride and sulfide ions were measured as a function of immersion time (Fig. 6(a)). Both F^- and SO_4^{2-} concentrations declined rapidly for 5 min (Fig. 6(a)). The synthesized product HTlc-Cl_pH10 eliminated approximately 30% of F^- (from 200 ppm to

140 ppm) and 35% of SO_4^{2-} (from 200 ppm to 130 ppm) in 5 min. This period was followed by a slower reduction of the ion concentrations to 110 ppm (F^-) and 105 ppm (SO_4^{2-}) in 60 min. Figure 6(b) demonstrates that adding 0.7 g HTlc-Cl_pH10 to the solution reduced the concentrations of both fluoride and sulfide anions to 50% of their original values (from 200 ppm to 100 ppm) in 5 min. An F^- concentration of 80 ppm remained in the solution at 60 min, representing a final reduction of F^- concentration of about 60%; a SO_4^{2-} concentration of only 25 ppm remained at this time, representing a reduction of around 88%. The affinity of SO_4^{2-} toward the interlayer of HTlc is stronger than that of F^- ,¹⁴ which fact probably explains why more SO_4^{2-} than F^- is absorbed. These results confirm that the waste metal conversion process changed the unrecyclable Mg scrap into Mg–Al–Cl HTlc powder, which can be potentially used to treat wastewater.

3.2 Chemical conversion surface treatment of Mg flake (flash) scraps and characterization of the surface coating

3.2.1 Mg-Al-Cl HTlc coating on surface of flake scraps. When 1.5 g of flash scraps (AM60 and AZ91 flash scraps) is added to the NaCl_pH 1.5 solution, the pH increases rapidly from 1.5 to approximately 9 in 30 min and to around 10 in 60 min. Magnesium reacts with the aqueous solution at $\text{pH} \leq 11.5$, as described by reaction (1),⁴⁵ which is responsible for the dramatic increase in the pH of the solution immediately following the immersion of magnesium scraps in the NaCl_pH 1.5 solution.

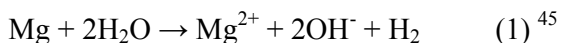


Figure 7 presents the GAXRD patterns of the primitive flash scraps and of those that were treated in NaCl_pH 1.5 solution for 30 min. Figure 7(a) displays the X-ray patterns of the AM60 scraps before and after the treatment, indicating that AM60-HTlc^{30min} yields the X-ray intensity

peaks of Mg-Al HTlc (peaks A). Importantly, the X-ray peaks of the HTlc coating had a large half-width unlike those of crystalline Mg (peaks B) in Fig. 7(a). The present authors' earlier study³³ found that the HTlc coating contained Mg-Al-CO₃ HTlc precursor when the half-width of the HTlc X-ray peak was large. The precursor contained excess Al.³³ Figure 7(b) presents the patterns of AZ91 and the AZ91_HTlc^{30min}, obtained after the AZ91 scraps were treated in NaCl_pH 1.5 solution for 30 min. Similarly, the X-ray peaks of the HTlc on AZ91D (peaks A in Fig. 7(b)) had a relatively large half-width. Figure 8 presents the FT-IR spectra of the AM60_HTlc^{30min} and AZ91_HTlc^{30min} samples. A broad absorption band at ~3442 cm⁻¹ corresponds to the H-bond stretching vibrations of the hydroxyl group in the hydroxide layer.⁴⁶ The absorption band at ~1632 cm⁻¹ is attributed to the bending motion of the water in the interlayer.⁴⁷ The band at ~1440 cm⁻¹ is weak, indicating the presence of amorphous carbonate.³³ The absorption band at ~1370 cm⁻¹ is characteristic of the asymmetric stretching mode of CO₃²⁻ (ν₃). The absorption bands at ~1370 cm⁻¹ and ~1440 cm⁻¹ are weak, suggesting that the interlayer of HTlc contained only a few carbonate ions. The band at ~585 cm⁻¹ is associated with the Al-OH translation mode in HTlc.⁴⁸ The band at ~420 cm⁻¹ is associated with various lattice vibrations of the metal hydroxide sheets in the HTlc material.⁴⁹ However, FT-IR did not detect the Cl⁻ in the spaces among the hydroxide sheets). Figures 9 (a) and (b) present the EDS spectra of the AM60_HTlc^{30min} and AZ91_HTlc^{30min} samples, which include Cl peaks. Notably, the EDS spectra of neither of these two samples included an Na peak, revealing that the Cl signal was not associated with NaCl. The table in Fig. 9 reveals that the Al concentration in AM60_HTlc^{30min} was ~3.63 wt.% and the Cl concentration therein was ~2.55 wt.%, as determined by SEM/EDS (EDS scanning area: 30 × 30 μm²). The Al concentration in AZ91_HTlc^{30min} was ~8.21 wt.% and the Cl concentration therein was ~5.85 wt.% (EDS scanning area: 30 × 30 μm²). The Al and Cl concentrations of AZ91_HTlc^{30min} exceeded those of AM60_HTlc^{30min}. The chemical reaction (corrosion) of the Mg-Al alloy scrap in NaCl_pH1.5 aqueous yielded Mg²⁺ and Al³⁺ to the solution. The formation of cationic layers requires a high

enough concentration of the Al^{3+} cations, which replace some of the Mg^{2+} at the octahedral lattice sites of magnesium hydroxide. The relevant results (Fig. 7 and Fig. 8) confirm that the magnesium alloy (AM60) that contains less aluminum than AZ91 could also develop an Mg–Al–Cl HTlc coating on AM60.

Figure 10(a) presents the SEM observations of the surfaces of the as-received AM60 scraps (top photograph in Fig. 10(a)) and AM60_HTlc^{30min} (bottom photograph in Fig. 10(a)). Figure 10(b) shows the surface microstructures of the as-received AZ91 scrap (top photograph in Fig. 10(b)) and AZ91_HTlc^{30min} (bottom photograph in Fig. 10(b)). Solidification microstructures of the as-received AM60 (top photograph in Fig. 10(a)) and AZ91 (top photograph in Fig. 10(b)) were observed. The flash scraps strongly reacted with NaCl_pH 1.5 aqueous, rapidly increasing the pH of the solution from 1.5 to ~9 in 20 min, consistent with the reaction equation (1). The post-treated surface microstructures of AM60_HTlc^{30min} and AZ91_HTlc^{30min} (shown in the bottom micrographs of Fig. 10(a) and (b)) revealed conventional HTlc structures with fine and upstanding platelet-like HTlc disks.

3.2.2 Activity of the HTlc film on Mg alloy flake scrap – the capacity to uptake F^- from waste

solution. Figure 11(a) shows the removal of F^- by AM60_HTlc^{30min} and AZ91_HTlc^{30min} in an aqueous solution of 100 ppm fluoride. AM60_HTlc^{30min} (1.5 g) reduced the concentration of fluoride from 100 ppm to 77.3 ppm in 10 min and to 71.2 ppm in 60 min, while 1.5 g AZ91_HTlc^{30min} reduced the concentration of fluoride from 100 ppm to 64.2 ppm in 10 min and to 53.7 ppm in 60 min. Figure 11(b) displays the FT-IR spectra of the AM60_HTlc^{30min} and AZ91_HTlc^{30min} samples following the uptake of F^- . An intense and sharp absorption band at $\sim 1384 \text{ cm}^{-1}$ reveals that the fluoride ions were intercalated in the spaces between hydroxide sheets,⁵⁰ suggesting that AM60_HTlc^{30min} and AZ91_HTlc^{30min} exchanged Cl^- with F^- in the water.

Additionally, AM60-HTlc^{30min} and AZ91-HTlc^{30min} had F⁻ absorption bands with similar FT-IR intensities. That is, these two samples had similar anion-exchange capacities. However, since AZ91-HTlc^{30min} actually took up more F⁻ than AM60-HTlc^{30min} did (Fig. 11(a)), some other mechanism must have been responsible for the removal of F⁻ from solution.

Apart from the mechanism of interlayer anion-exchange, a hydrotalcite-like structure of an HTlc platelet has a high surface area that probably facilitates the adsorption of F⁻ ions on its surface. According to some investigations,^{51, 52} HTlcs can take up anion species from solution by three mechanisms – adsorption to the surface of HTlcs platelets, interlayer anion-exchange and reconstruction of the HTlc precursor. In the present work, the adsorption of F⁻ by HTlc platelets surface may have occurred when residual positive charges associated with Al³⁺ were present in the HTlc. These residual positive charges would have been balanced by F⁻ adsorption. Moreover, HTlcs may adsorb anion species from solution by the reconstruction of an HTlc precursor by the “memory effect”.^{51, 53} Li and Duan⁵¹ suggested that the “memory effect” of the HTlc precursor is one of its attractive features as an adsorbent of anionic species. Naime Filho *et al.*⁵³ studied the “memory effect” of the calcined HTlc precursor, and concluded that organic anions could be adsorbed outside the layers of the HTlc. In the present work, the as-synthesized AZ91-HTlc^{30min} and AM60-HTlc^{30min} contained an amorphous precursor, as revealed by the relatively large half-widths of the HTlcs X-ray peaks (Fig. 7, mentioned in Section 3.2). In the experiments, AZ91-HTlc^{30min} took up more F⁻ from solution than did the AM60-HTlc^{30min} (Fig. 11), probably because the former sample exhibited a higher sorption capacity for F⁻. More experimental results concerning adsorption by HTlc, and a related explanation, will be presented later.

3.2.3 Improving the Activity of the HTlc film on AM60 flake scrap. For the purpose to improve uptake of F⁻ by Mg–Al–Cl HTlc coating on AM60 scrap, two aqueous solutions

$\text{AlCl}_3^{0.02}\text{-NaCl-pH1.5}$ and $\text{AlCl}_3^{0.22}\text{-NaCl-pH1.5}$ were prepared by adding 0.02 g AlCl_3 and 0.22 g AlCl_3 , respectively, to 200 ml of NaCl-pH1.5 aqueous. Approximately 1.5 g AM60 of flash scrap was respectively immersed in the $\text{AlCl}_3^{0.02}\text{-NaCl-pH 1.5}$ and the $\text{AlCl}_3^{0.22}\text{-NaCl-pH 1.5}$ solutions. The change of the pH of $\text{AlCl}_3^{0.02}\text{-NaCl-pH 1.5}$ solution as a function of immersion time was similar to that of NaCl-pH 1.5 solution to which was added AM60 (as described previously in Section 3.2). The pH of the $\text{AlCl}_3^{0.02}\text{-NaCl-pH 1.5}$ solution increased from pH 1.5 to pH 9 in 30 min and to approximately pH 10 in 60 min. However, the pH of $\text{AlCl}_3^{0.22}\text{-NaCl-pH 1.5}$ as a function of time following the immersion of AM60 scrap therein increased from 1.5 to ~ 4.3 in 20 min, after which it was reasonably constant until the immersion time reached 60 min. Thereafter, pH increased to ~ 9 as the immersion time increased to 120 min. Figures 12 (a) ~ (c) show the surface microstructures of $\text{AM60_HTlc}^{30\text{min}}$, $\text{AM60}^{0.02}\text{-HTlc}^{30\text{min}}$ and $\text{AM60}^{0.22}\text{-HTlc}^{30\text{min}}$. $\text{AM60_HTlc}^{30\text{min}}$ and $\text{AM60}^{0.02}\text{-HTlc}^{30\text{min}}$ (Fig.12 (a) and (b)) had a typical microstructure of a platelet-like HTlc. The size of the platelets of $\text{AM60}^{0.02}\text{-HTlc}^{30\text{min}}$ (Fig. 12 (b)) was approximately the same as that of $\text{AM60_HTlc}^{30\text{min}}$ platelets (Fig. 12 (a)), as shown in the insets. Figure 12 (c) presents the surface microstructure of $\text{AM60}^{0.22}\text{-HTlc}^{30\text{min}}$, which contains very fine HTlc platelets (~ 100 nm wide (see the inset in Fig. 12 (c))). Figure 12(d) presents the GAXRD patterns of $\text{AM60_HTlc}^{30\text{min}}$, $\text{AM60}^{0.02}\text{-HTlc}^{30\text{min}}$ and $\text{AM60}^{0.22}\text{-HTlc}^{30\text{min}}$. All of the patterns included X-ray peaks of Mg–Al HTlc (denoted as A). The X-ray peaks of the HTlc in the three samples had larger half-widths than the sharp peaks of crystalline Mg (denoted as B). Evidently, the half-width of the HTlc peak from $\text{AM60}^{0.22}\text{-HTlc}^{30\text{min}}$ was larger than those of the HTlc peaks from the other two samples (Fig. 12(d)), suggesting that $\text{AM60}^{0.22}\text{-HTlc}^{30\text{min}}$ contained the most HTlc precursor.³³

Figure 13 (a) shows the uptake of F^- by $\text{AM60_HTlc}^{30\text{min}}$, $\text{AZ91_HTlc}^{30\text{min}}$, $\text{AM60}^{0.02}\text{-HTlc}^{30\text{min}}$ and $\text{AM60}^{0.22}\text{-HTlc}^{30\text{min}}$ from aqueous 100 ppm fluoride. Figure 13(a) re-plots the data for $\text{AM60_HTlc}^{30\text{min}}$ in Fig. 11(a). $\text{AM60_HTlc}^{30\text{min}}$ (1.5 g) reduced the concentration of

fluoride ions from 100 ppm to 77.3 ppm in 10 min and to 71.2 ppm in 60 min. The data for AZ91_HTlc^{30min} (presented in Fig. 11 (a)), also shown in this figure for comparison, demonstrate that AZ91_HTlc^{30min} reduced the concentration of fluoride ions from 100 ppm to 64.2 ppm in 10 min and to 53.7 ppm in 60 min. AM60^{0.02}_HTlc^{30min} reduced the concentration of fluoride ions from 100 ppm to 71 ppm in 10 min and to 65.2 ppm in 60 min. AM60^{0.22}_HTlc^{30min} reduced the concentration of fluoride ions from 100 ppm to 57 ppm in 10 min and to 35.9 ppm in 60 min. The ability of AM60^{0.02}_HTlc^{30min} to take up F⁻ exceeded that of AM60_HTlc^{30min}. Among these HTlc samples, AM60^{0.22}_HTlc^{30min} had the highest ability to take up F⁻. Based on the above results, adding AlCl₃ to NaCl_pH 1.5 aqueous to coat AM60 scraps with HTlc improved their capacity to take up F⁻. Figure 13 (b) displays the FT-IR spectra of the AM60_HTlc^{30min}, AM60^{0.02}_HTlc^{30min} and AM60^{0.22}_HTlc^{30min} samples after their uptake of F⁻. An intense band at ~1384 cm⁻¹ associated with the signal from the intercalated F⁻ indicates that the fluoride ions occupied the spaces between hydroxide sheets.⁵⁰ According to Fig. 13 (b), all of the HTlc samples had absorption bands at ~1384 cm⁻¹ of similar intensities. FT-IR data suggest that the three samples AM60_HTlc^{30min}, AM60^{0.02}_HTlc^{30min} and AM60^{0.22}_HTlc^{30min} exhibited almost identical anion-exchangeabilities with respect to the intercalation of F⁻ in HTlc interlayers. However, the amounts of F⁻ taken up by pairs of HTlc-coated samples in the 60 min-long experiment follow the order AM60_HTlc^{30min} < AM60^{0.02}_HTlc^{30min} < AM60^{0.22}_HTlc^{30min}. Thus, the results of FT-IR analysis did not match the measured uptakes of F⁻ which are presented in Fig. 13 (a).

In Mg-Al hydrotalcite, each Al³⁺ that occupies an Mg²⁺ lattice site generates an extra positive charge in the brucite layer of the hydrotalcite. The extra positive charge was denoted as Al_{Mg}⁺, representing the fact that one Al ion occupies one Mg lattice site, resulting in one positive charge. As a result, the cationic brucite layers were formed herein, and then intercalating Cl ions balanced the positive charges. However, the cationic brucite layers would not have been well balanced if

excess Al^{3+} had been presented in the cationic layers or insufficient Cl^- had been intercalated. EDS surface scanning analysis was performed to determine the atomic percentages of Al and Cl on Mg-Al-Cl HTlc coating. All of the Al^{3+} in the Mg-Al-Cl HTlc structure is assumed to have occupied Mg lattice sites, so Al_{Mg}^+ stands for Al^{3+} . In this study, “residue positive charge (RPC)” is defined as $[\text{Al}_{\text{Mg}}^+(\text{at}\%) - \text{Cl}^-(\text{at}\%)]$. When the RPC value exceeds zero, the HTlc material not only exhibits anion-exchangeability but also the residual positive charges may be balanced by the adsorption of F^- . When HTlc does not have a net residual positive charge (i.e., RPC equals zero), the HTlc exhibits only anion-exchangeability. Figure 14(a), based on the data in Fig. 11 (a) and 13 (a), plots the F^- taken up from solution (ppm) against RPC $[\text{Al}_{\text{Mg}}^+(\text{at}\%) - \text{Cl}^-(\text{at}\%)]$. The three linear lines in Fig. 14(a) correspond to immersion times of 10 min, 30 min and 60 min. The amount of F^- taken up is proportional to the RPC value (Fig. 14(a)). The concentration of F^- taken up is extrapolated to be ~ 20 ppm (at an immersion time of 10 min), ~ 20 ppm (30 min) and ~ 21 ppm (60 min) for HTlc samples without any residual positive charge (RPC = 0) (Fig. 14(a)). The extrapolated values from the three fitted lines were almost equal, suggesting that the anion-exchangeability of the three HTlc samples herein was approximately 20 ppm. This result is consistent with the FT-IR results for the HTlc samples (Fig. 13(b)), which revealed that they had similarly intense peaks associated with the intercalated F^- . Figure 14(b) schematically depicts the linear relationship (thick blue line) between the concentration of F^- taken up from solution vs. RPC. A dotted line passes through the point where the blue line intercepts the Y-axis at RPC = 0. The dotted line parallel to the X-axis shows that the samples with different RPC values exhibit the same F^- intercalation ability. AM60_HTlc^{30min} had a low RPC value (Figs. 14(a)), having taken up a relatively small amount of F^- from solution. As schematically depicted in Fig. 14(b), a small amount of F^- was taken up by the sample with a low RPC. As shown in Fig. 14(b), in the sample with the low RPC, anion intercalation was the dominant mechanism by which F^- was taken up from solution. For AM60^{0.22}_HTlc^{30min} (high RPC

value), the main mechanism involved the precursor of HTlc on the surface of the sample associated with the broad X-ray peaks from HTlc (see the bottom pattern in Fig. 12(d)). AM60^{0.22}_HTlc^{30min} had a high RPC value (Fig. 14(a)), and therefore took up a large amount of F⁻ from solution to balance those charges, both by simple surface adsorption and by adsorption outside the layers of HTlc during the reconstruction of the HTlc precursor. As schematically depicted in Fig. 14(b), surface sorption dominated the uptake of F⁻ from solution when the sample had high RPC.

In practice, all Mg-Al HTlc compounds could be used as catalysts. According to Choudary *et al.*⁵⁴ and Rousselot *et al.*,⁵⁵ Mg-Al HTlc^{54,55} and the compound that is formed by its calcination⁵⁵ at 450 °C exhibit favorable catalytic activity in the condensation of benzaldehyde and cyclohexanone, respectively. Accordingly, the present paper may support the development of a new method for treating waste magnesium scraps to turn them into a valuable resource.

4. Conclusions

1. Intermetallic compound Al₁₂Mg₁₇ can be produced by melting bulk-type Mg waste and Al waste in a furnace in air. The compound was weak and brittle, which was easily to be pulverized and powdered. The Al₁₂Mg₁₇ powder can be dissolved by hydrolysis in aqueous HCl acid, easily forming an ionic solution of Al³⁺, Mg²⁺ and the anion Cl⁻. Mg-Al-Cl HTlc can be produced in the ionic aqueous solution at room temperature when the alkalinity of the solution was increased to pH 10, and the pH 10 of the solution was maintained for approximately 10 min. Experimental conditions that maximized the yield of Mg-Al-X HTlc, converting all of the Al³⁺ and Mg²⁺ ions into the valuable HTlc, were identified.
2. The above method can be extended to the formation of a wide range of Mg-Al-X HTlcs (X= NO₃⁻ or SO₄²⁻, etc.). By simply adding Al₁₂Mg₁₇ powder to particular inorganic acids (such as

HNO₃ and H₂SO₄), solutions that contain Al³⁺, Mg²⁺ and the specified anion (such as NO₃⁻ or SO₄²⁻) can be formed. We have confirmed that Mg–Al–X HTlcs (X= NO₃⁻ and SO₄²⁻) were formed when the solution was made alkaline and remained so for an extended period.

3. A novel method was found to directly develop an Mg–Al–Cl HTlc thin film on the surfaces of flake–type Mg–Al alloy scrap, to enable the metallic waste to be reusable. Aqueous 3.5 wt. % NaCl (through which Ar was bubbled) at pH 1.5 was the base solution for treating the surfaces of the scraps. The surface of the Mg–Al alloy flakes in aqueous solution was important, not only in providing Mg²⁺ and Al³⁺ (by heavy corrosion) but also in increasing the pH of the solution, both of which processes favored the formation of Mg–Al–Cl HTlc film. In practice, HTlc-coated Mg flash (flake) scraps can, for example, take up enough fluoride ions from waste water to reduce greatly the fluoride concentration therein.
4. Adding AlCl₃ to the base solution generated a new aqueous solution for recycling Mg alloy flake scraps. Al³⁺ must be added to the base solution to supply sufficient Al³⁺ to form the Mg–Al–Cl hydrotalcite-like coating on the Mg alloy scraps. Additionally, the new aqueous (pH 1.5) solution with the greater Al³⁺ concentration can form an Mg–Al–Cl HTlc film with a much higher F⁻–uptake ability.
5. Herein, residual positive charge of the Mg–Al–Cl HTlc film was defined as the atomic percent of aluminum (Al³⁺) minus the atomic percent of chloride (Cl⁻). It was found that the amount of F⁻ that was taken up by the HTlc film was proportional to the value of the residual positive charges of the film. Anion surface sorption was found to be the dominant mechanism by which the Mg–Al–Cl HTlc film removed most of the anionic contaminant from solution.

Acknowledgements

This study was funded by a Ministry of Education grant (Taiwan, Republic of China) under the ATU plan and the National Science Council of Taiwan (NSC 98-2221-E-005-028 and NSC 101-2221-E-005-027-MY3). The authors are grateful for their support.

Notes and References

^a *Department of Materials Science and Engineering, National Chung Hsing University, 250 kuo kuang Rd., Taichung 402, Taiwan, ROC.*

^b *Green Energy and Environment Research Laboratories, Industrial Technology Research Institute, 195 Sec. 4, Chung-Hsing Road, Hsin-Chu 31040, Taiwan, ROC*

* *Corresponding author*

Email: jyuan@dragon.nchu.edu.tw

Tel.: +886-4-22854913

Fax: +886-4-22857017

REFERENCES

1. H. Komiyama and S. Kraines, *Vision 2050: Roadmap for a Sustainable Earth*, Springer, 2008.
2. S. Ehrenberger and H. Friedrich, *JOM*, 2013, **65**, 1303-1309.
3. E. Daniels, J. Carpenter, Jr., C. Duranceau, M. Fisher, C. Wheeler and G. Winslow, *JOM*, 2004, **56**, 28-32.
4. M. Kulekci, *Int J Adv Manuf Technol*, 2008, **39**, 851-865.
5. C. Mendis and A. Singh, *JOM*, 2013, **65**, 1283-1284.
6. D. Fechner, C. Blawert, N. Hort, H. Dieringa and K. U. Kainer, *Materials Science and Engineering: A*, 2013, **576**, 222-230.
7. A. Javaid, E. Essadiqi, S. Bell and B. Davis, *Magnesium technology*, 2006, 7-12.
8. C. Blawert, D. Fechner, D. Höche, V. Heitmann, W. Dietzel, K. U. Kainer, P. Živanović, C. Scharf, A. Ditze, J. Gröbner and R. Schmid-Fetzer, *Corrosion Science*, 2010, **52**, 2452-2468.
9. a. A. Ditze and C. Scharf, *Recycling of Magnesium*, Papierflieger-Verlag, 2008.; b. S. Das, *Recycling and life cycle issues for lightweight vehicles*, in "*Materials, design and manufacturing for lightweight vehicles*", edited by P. K. Mallick, Woodhead Publishing Limited and CRC Press LLC, 2010.
10. I. Polmear, *Light Alloys: From Traditional Alloys to Nanocrystals*, Elsevier Science, 2005.
11. J. Milroy, S. Hinduja and K. Davey, *Proceedings of the Institution of Mechanical Engineers, Part C: Journal of Mechanical Engineering Science*, 1998, **212**, 197-215.
12. J.-Y. Uan, M.-C. Lin, C.-Y. Cho, K.-T. Liu and H.-I. Lin, *International Journal of Hydrogen Energy*, 2009, **34**, 1677-1687.

13. F. Cavani, F. Trifirò and A. Vaccari, *Catalysis Today*, 1991, **11**, 173-301.
14. S. Miyata, *Clays and Clay Minerals*, 1983, **31**, 305-311.
15. U. Olsbye, D. Akporiaye, E. Rytter, M. Rønnekleiv and E. Tangstad, *Applied Catalysis A: General*, 2002, **224**, 39-49.
16. H. C. Greenwell, P. J. Holliman, W. Jones and B. V. Velasco, *Catalysis Today*, 2006, **114**, 397-402.
17. U. Costantino, F. Marmottini, M. Nocchetti and R. Vivani, *European Journal of Inorganic Chemistry*, 1998, **1998**, 1439-1446.
18. K. Okamoto, N. Iyi and T. Sasaki, *Appl Clay Sci*, 2007, **37**, 23-31.
19. M.-C. Lin, F.-T. Chang and J.-Y. Uan, *Journal of Materials Chemistry*, 2010, **20**, 6524-6530.
20. J. Zhao, M. Shao, D. Yan, S. Zhang, Z. Lu, Z. Li, X. Cao, B. Wang, M. Wei, D. G. Evans and X. Duan, *Journal of Materials Chemistry A*, 2013, **1**, 5840-5846.
21. Y. Gao, J. Wu, Z. Zhang, R. Jin, X. Zhang, X. Yan, A. Umar, Z. Guo and Q. Wang, *Journal of Materials Chemistry A*, 2013, **1**, 9928-9934.
22. B. M. Choudary, S. Madhi, N. S. Chowdari, M. L. Kantam and B. Sreedhar, *Journal of the American Chemical Society*, 2002, **124**, 14127-14136.
23. K. Y. Park, J. H. Song, S. H. Lee and H. S. Kim, *Environmental Engineering Science*, 2010, **27**, 805-810.
24. M. Trikeriotis and D. F. Ghanotakis, *International Journal of Pharmaceutics*, 2007, **332**, 176-184.
25. Y. Gao, Z. Zhang, J. Wu, X. Yi, A. Zheng, A. Umar, D. O'Hare and Q. Wang, *Journal of Materials Chemistry A*, 2013, **1**, 12782-12790.
26. M.-C. Lin, F.-T. Chang and J.-Y. Uan, *Journal of Materials Chemistry A*, 2013, **1**, 14773-14782.

27. B. M. Choudary, B. Bharathi, C. V. Reddy, M. L. Kantam and K. V. Raghavan, *Chemical Communications*, 2001, 1736-1737.
28. B. M. Choudary, T. Someshwar, M. Lakshmi Kantam and C. Venkat Reddy, *Catalysis Communications*, 2004, **5**, 215-219.
29. S. Miyata, *Clays and Clay Minerals*, 1975, **23**, 369-375.
30. N. Iyi, T. Matsumoto, Y. Kaneko and K. Kitamura, *Chemistry of Materials*, 2004, **16**, 2926-2932.
31. J. K. Lin, C. L. Hsia and J. Y. Uan, *Scripta Materialia*, 2007, **56**, 927-930.
32. J. K. Lin and J. Y. Uan, *Corrosion Science*, 2009, **51**, 1181-1188.
33. J.-K. Lin, K.-L. Jeng and J.-Y. Uan, *Corrosion Science*, 2011, **53**, 3832-3839.
34. J. Chen, Y. Song, D. Shan and E.-H. Han, *Corrosion Science*, 2012, **63**, 148-158.
35. F. Zhang, Z. G. Liu, R. C. Zeng, S. Q. Li, H. Z. Cui, L. Song and E. H. Han, *Surface Coating and Technology*, 2014, DOI: 10.1016/j.surfcoat.2014.07.017.
36. T. Ishizaki, S. Chiba, K. Watanabe and H. Suzuki, *Journal of Materials Chemistry A*, 2013, **1**, 8968-8977.
37. X.L. Wang, J.P. Tu, P. L. Zhang, X.B. Zhang, C.P. Chen, and X.B. Zhao, *Int. J. Hydrogen Energy*, 2007, **32**, 3406-3410.
38. A. Tsujimura, M. Uchida and A. Okuwaki, *Journal of Hazardous Materials*, 2007, **143**, 582-586.
39. Z. P. Xu, T. L. Walker, K.-I. Liu, H. M. Cooper, G. M. Lu and P. F. Bartlett, *International journal of nanomedicine*, 2007, **2**, 163-174.
40. A. Violante, M. Pucci, V. Cozzolino, J. Zhu and M. Pigna, *Journal of Colloid and Interface Science*, 2009, **333**, 63-70.
41. L. Lv, J. He, M. Wei, D. G. Evans and X. Duan, *Journal of Hazardous Materials*, 2006, **133**, 119-128.

42. M. Adachi-Pagano, C. Forano and J.-P. Besse, *Journal of Materials Chemistry*, 2003, **13**, 1988-1993.
43. H. Liu, J. Hu, J. Xu, Z. Liu, J. Shu, H. K. Mao and J. Chen, *Phys Chem Minerals*, 2004, **31**, 240-246.
44. R. L. Frost, J. T. Kloprogge, S. C. Russell and J. L. Szetu, *Applied Spectroscopy*, 1999, **53**, 423-434.
45. M. Pourbaix, *Atlas of electrochemical equilibria in aqueous solutions*, National Association of Corrosion Engineers, 1974.
46. M. del Arco, S. Gutierrez, C. Martin and V. Rives, *Physical Chemistry Chemical Physics*, 2001, **3**, 119-126.
47. P. Zhang, G. Qian, H. Shi, X. Ruan, J. Yang and R. L. Frost, *Journal of Colloid and Interface Science*, 2012, **365**, 110-116.
48. F. Millange, R. I. Walton and D. O'Hare, *Journal of Materials Chemistry*, 2000, **10**, 1713-1720.
49. F. R. Costa, A. Leuteritz, U. Wagenknecht, D. Jehnichen, L. Häußler and G. Heinrich, *Appl Clay Sci*, 2008, **38**, 153-164.
50. N. Viswanathan and S. Meenakshi, *Appl Clay Sci*, 2010, **48**, 607-611.
51. F. Li and X. Duan, in *Layered double hydroxides*, Springer, 2006, pp. 193-223.
52. J. F. N. Filho and J. Barros Valim, *Journal of Physics and Chemistry of Solids*, 2010, **71**, 620-623.
53. J. F. Naime Filho, F. Silvério, M. J. dos Reis and J. B. Valim, *J Mater Sci*, 2008, **43**, 6986-6991.
54. B. M. Choudary, M. Lakshmi Kantam, V. Neeraja, K. Koteswara Rao, F. Figueras and L. Delmotte, *Green Chemistry*, 2001, **3**, 257-260.
55. I. Rousselot, C. Taviot-Guého and J. P. Besse, *International Journal of Inorganic*

Materials, 1999, **1**, 165-174.

Figure captions

Fig. 1 (a) AZ91 scrap of commercial die-cast; (b) Al scrap of cable wire for electric transition; (c) $\text{Al}_{12}\text{Mg}_{17}$ cast ingot made from commercial magnesium alloy scrap and aluminum alloy scrap; (d) X-ray powder diffraction pattern of cast ingot.

Fig. 2 (a) Smash-down pieces of $\text{Al}_{12}\text{Mg}_{17}$ from cast ingot, which is not pyrophoric and can be handled in air; (b) the ground powder of $\text{Al}_{12}\text{Mg}_{17}$.

Fig. 3 Mg alloys die casting flash scraps that currently can not be recycled economically: (a) AM60 scrap; (b) AZ91 scrap. The thin flash scraps easily to be broken down to small pieces, as shown in (c).

Fig. 4 (a) X-ray powder diffraction pattern of Mg-Al-Cl HTlc; (b) FT-IR spectra of Mg-Al-Cl HTlc; (c) EDS spectrum of Mg-Al-Cl HTlc at the condition of pH 10; (d) microstructure of Mg-Al-Cl HTlc, showing nanoplatelets.

Fig. 5 (a) Mg^{2+} and Al^{3+} concentrations in the residual solutions after each of the HTlc synthesization under different pH conditions; (b) Weight (g) of the synthetic product of Mg-Al-Cl HTlc under different pH.

Fig. 6 Fluoride and sulfide absorption by HTlc-Cl_pH10 (a) 0.35g; (b) 0.7g in the industrial waste water solution.

Fig. 7 GAXRD patterns of flash scraps and the scraps treated in NaCl_pH 1.5 solution for 30 min: (a) AM60 and AM60_HTlc^{30 min}; (b) AZ91 and AZ91_HTlc^{30 min}.

Fig. 8 FT-IR spectra for AM60_HTlc^{30 min} and AZ91_HTlc^{30 min}.

Fig. 9 EDS spectrum for (a) AM60_HTlc^{30 min} and (b) AZ91_HTlc^{30 min} (EDS scanning area: 30 × 30 μm²), with a table showing Mg, Al and Cl compositions (wt.%) of the HTlc film on AM60_HTlc^{30 min} and AZ91_HTlc^{30 min}.

Fig. 10 SEM surface morphologies of (a) the upper photo is original flash scrap AM60, while the lower photo is AM60_HTlc^{30 min}; (b) the upper photo is original flash scrap AZ91, while the lower photo is AZ91_HTlc^{30 min}.

Fig. 11 (a) Removal of fluoride ions (ppm) vs. immersion time in a fluoride aqueous solution (100 ppm) at pH 6 by 1.5 g AM60_HTlc^{30 min} and AZ91_HTlc^{30 min}; (b) IR spectra of AM60_HTlc^{30 min} and AZ91_HTlc^{30 min} after **60 min** of uptaking F⁻ at pH 6 ± 0.5.

Fig. 12 SEM surface morphologies: (a) AM60_HTlc^{30 min} (b) AM60^{0.02}_HTlc^{30 min} and (c) AM60^{0.22}_HTlc^{30 min} (d) GAXRD patterns: AM60_HTlc, AM60^{0.02}_HTlc and AM60^{0.22}_HTlc treated for 30 min.

Fig. 13 (a) Remove amount of fluoride ions (ppm) versus immersion time in a fluoride aqueous solution (100 ppm) at pH 6 by 1.5 g AM60_HTlc^{30 min}, AZ91_HTlc^{30 min}, AM60^{0.02}_HTlc^{30 min} and AM60^{0.22}_HTlc^{30 min}; (b) the samples' IR spectra after 60 min of F⁻ uptaking experiments.

Fig. 14 (a) F⁻ uptaken from solution (ppm) vs. RPC [Al_{Mg}⁺ (at%) – Cl⁻ (at%)]. Herein, RPC means residual positive charges; (b) a schematic plot showing that the mechanism of anion sorption became dominant as the RPC of the HTlc increased.

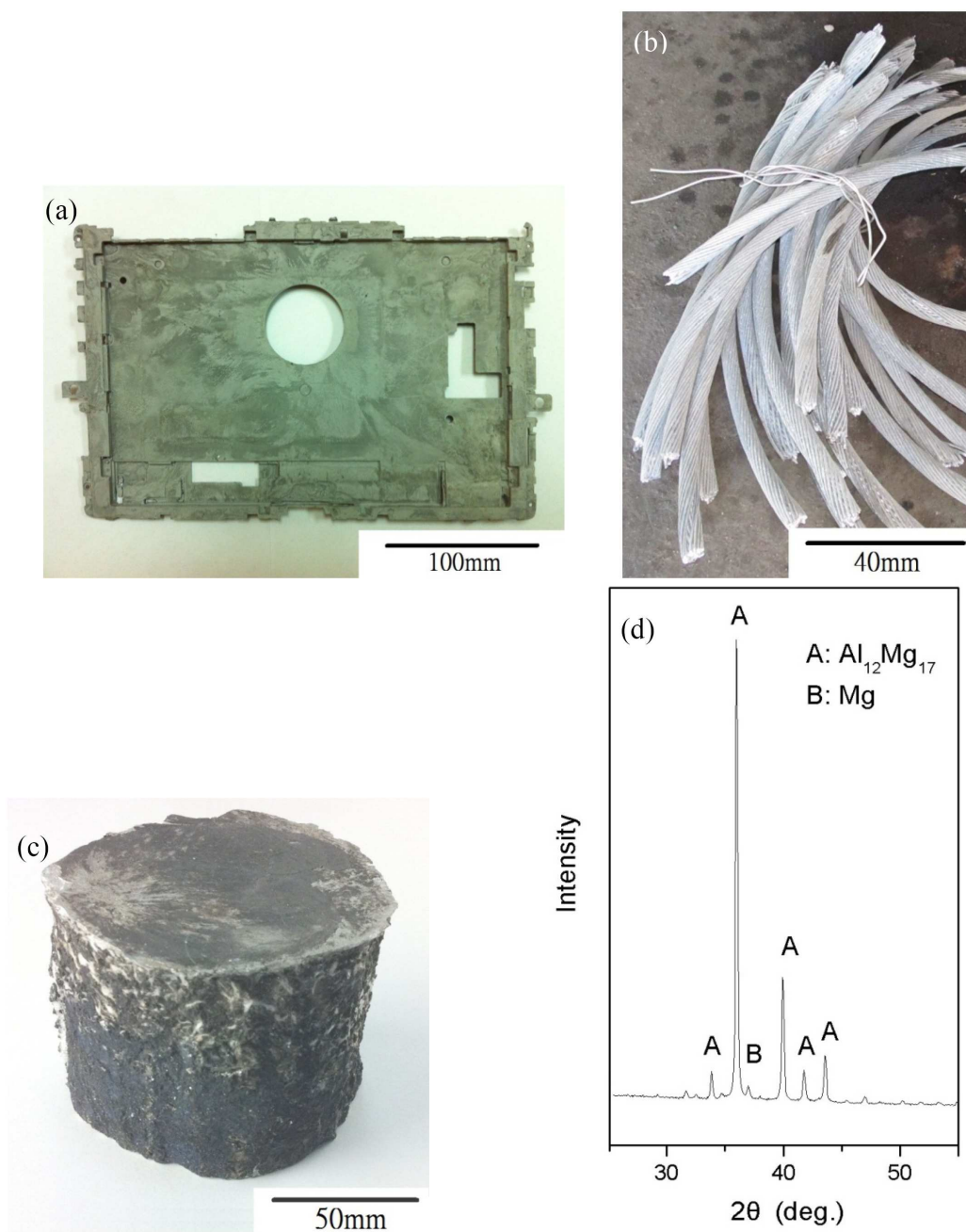


Fig. 1 (a) AZ91 scrap of commercial die-cast; (b) Al scrap of cable wire for electric transition; (c) $\text{Al}_{12}\text{Mg}_{17}$ cast ingot made from commercial magnesium alloy scrap and aluminum alloy scrap; (d) X-ray powder diffraction pattern of cast ingot.

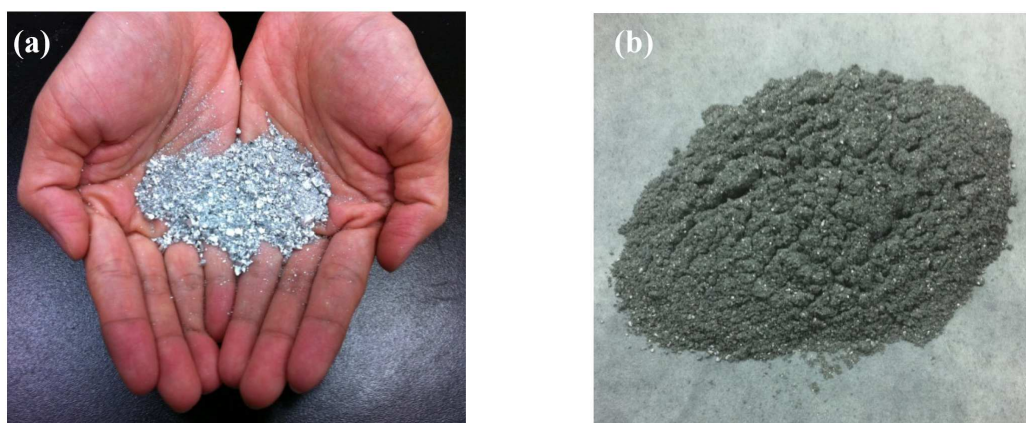


Fig. 2 (a) Smash-down pieces of $\text{Al}_{12}\text{Mg}_{17}$ from cast ingot, which is not pyrophoric and can be handled in air; (b) the ground powder of $\text{Al}_{12}\text{Mg}_{17}$.



Fig. 3 Mg alloys die casting flash scraps that currently can not be recycled economically: (a) AM60 scrap; (b) AZ91 scrap. The thin flash scraps easily to be broken down to small pieces, as shown in (c).

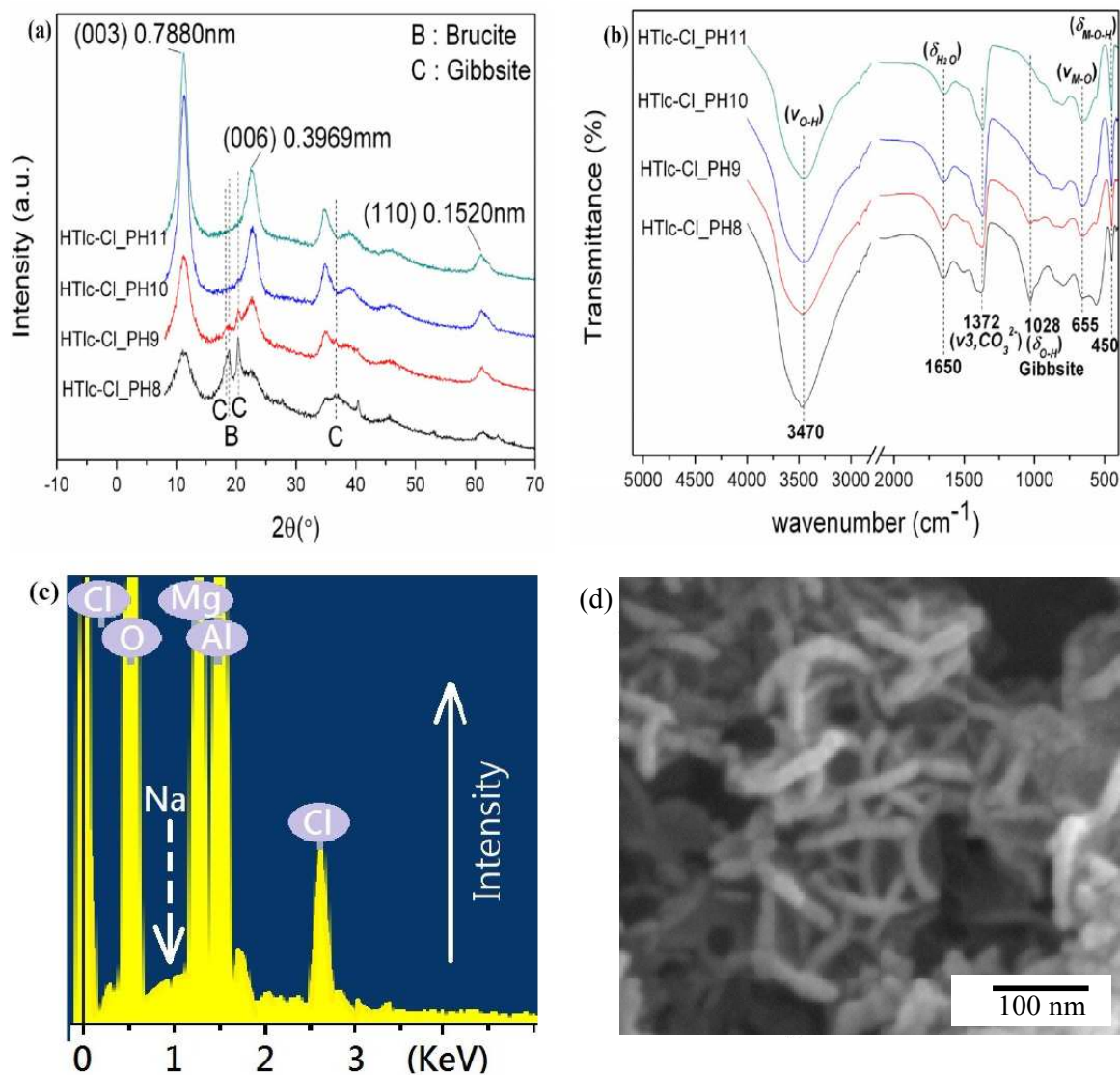


Fig. 4 (a) X-ray powder diffraction pattern of Mg-Al-Cl HTlc; (b) FT-IR spectra of Mg-Al-Cl HTlc; (c) EDS spectrum of Mg-Al-Cl HTlc at the condition of pH 10; (d) microstructure of Mg-Al-Cl HTlc, showing nanoplatelets.

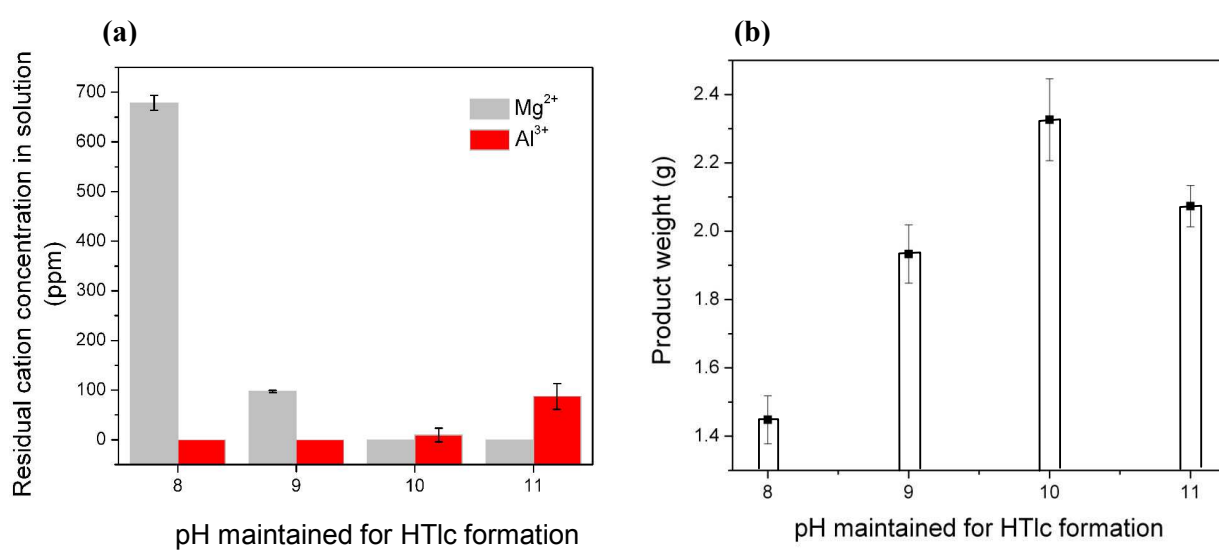


Fig. 5 (a) Mg^{2+} and Al^{3+} concentrations in the residual solutions after each of the HTlc synthesization under different pH conditions; (b) Weight (g) of the synthetic product of Mg-Al-Cl HTlc under different pH.

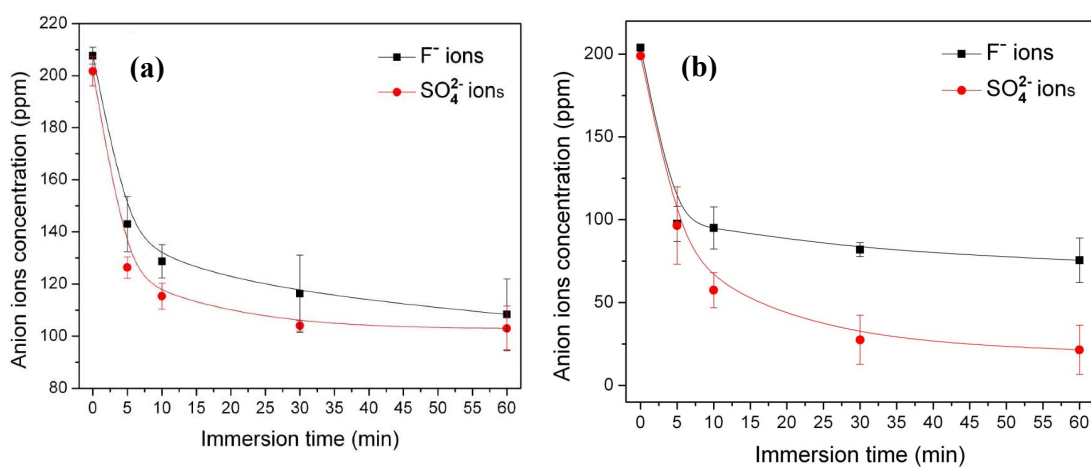


Fig. 6 Fluoride and sulfide absorption by HTlc-Cl_pH10 (a) 0.35g; (b) 0.7g in the industrial waste water solution.

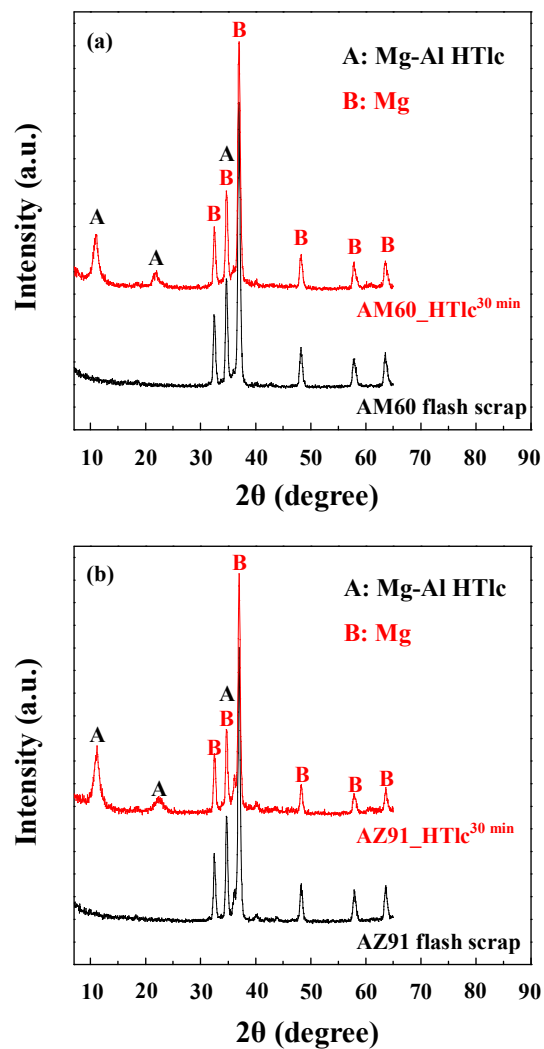


Fig. 7 GAXRD patterns of flash scraps and the scraps treated in NaCl pH 1.5 solution for 30 min: (a) AM60 and AM60_HTlc^{30 min}; (b) AZ91 and AZ91_HTlc^{30 min}.

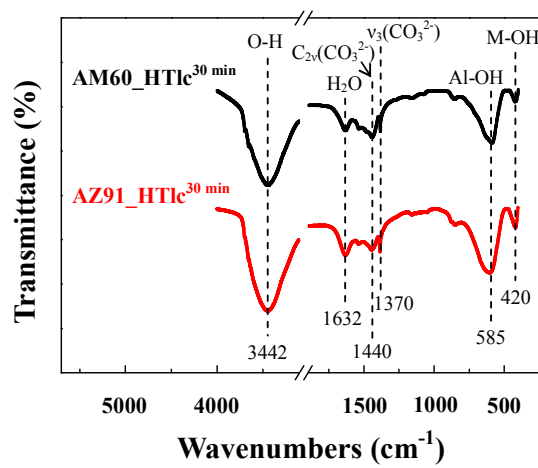
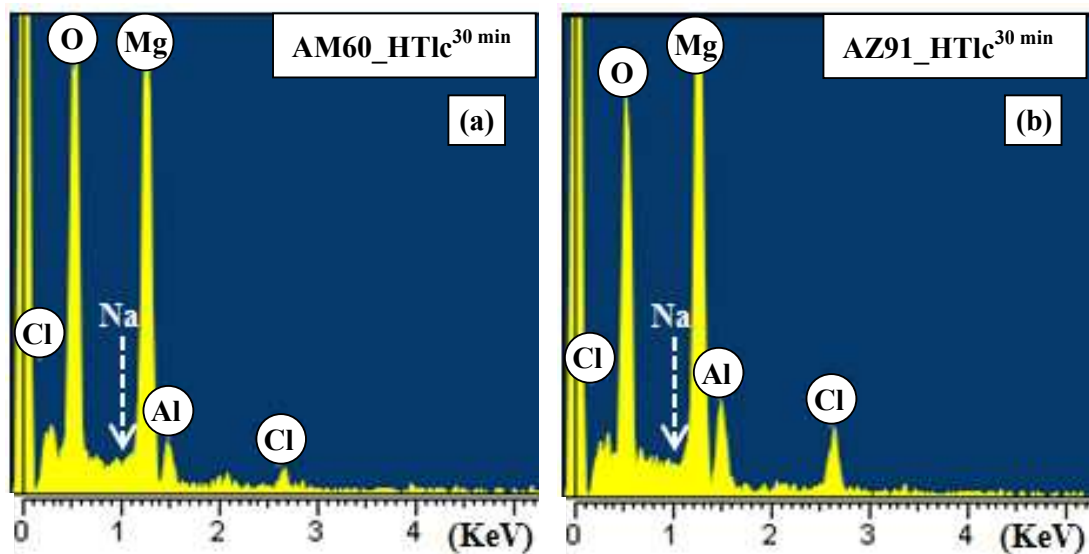


Fig. 8 FT-IR spectra for AM60_HTlc^{30 min} and AZ91_HTlc^{30 min}.



SEM/EDS \ wt.%	Mg	Al	AZ91_HTlc ^{30 min} Cl
AM60_HTlc ^{30 min}	34.52 ± 2.49	3.63 ± 1.51	2.55 ± 1.50
AZ91_HTlc ^{30 min}	30.20 ± 1.92	8.21 ± 1.06	5.85 ± 0.54

Fig. 9 EDS spectrum for (a) AM60_HTlc^{30 min} and (b) AZ91_HTlc^{30 min} (EDS scanning area: 30 × 30 μm²), with a table showing Mg, Al and Cl compositions (wt.%) of the HTlc film on AM60_HTlc^{30 min} and AZ91_HTlc^{30 min}.

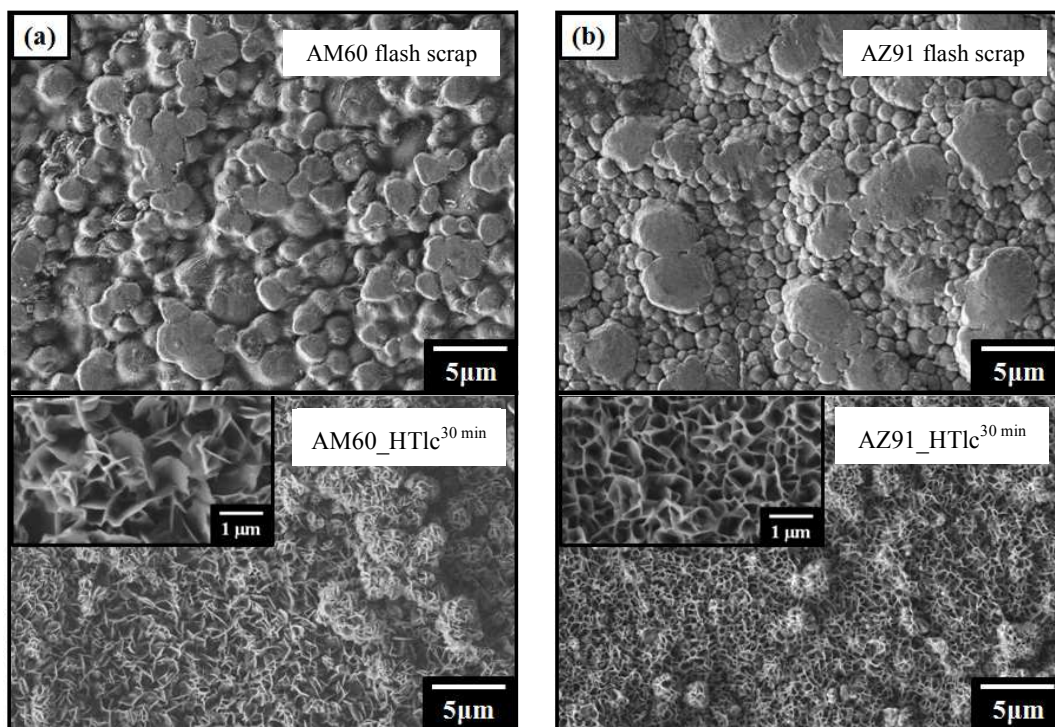


Fig. 10 SEM surface morphologies of (a) the upper photo is original flash scrap AM60, while the lower photo is AM60_HTlc^{30 min}; (b) the upper photo is original flash scrap AZ91, while the lower photo is AZ91_HTlc^{30 min}.

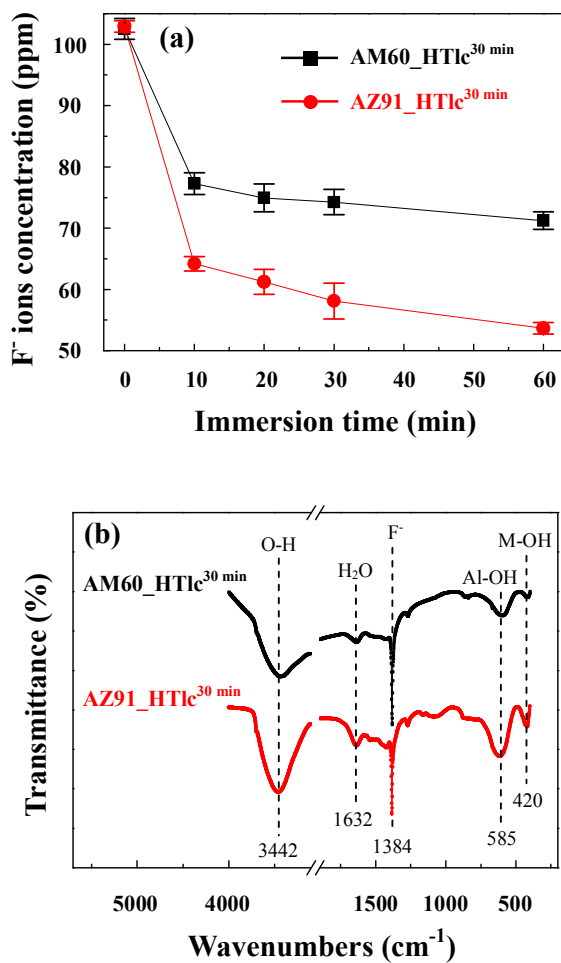


Fig. 11 (a) Removal of fluoride ions (ppm) vs. immersion time in a fluoride aqueous solution (100 ppm) at pH 6 by 1.5 g AM60_HTlc^{30 min} and AZ91_HTlc^{30 min}; (b) IR spectra of AM60_HTlc^{30 min} and AZ91_HTlc^{30 min} after 60 min of uptaking F⁻ at pH 6 ± 0.5.

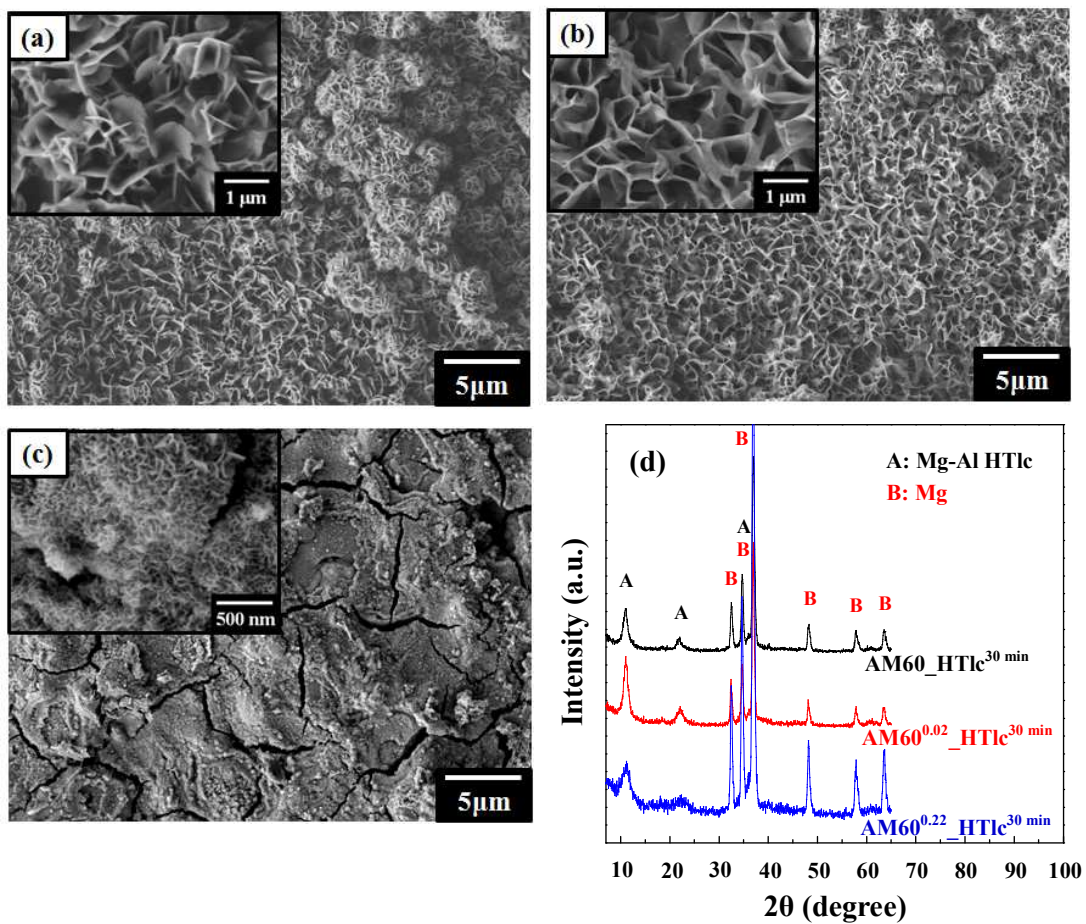


Fig. 12 SEM surface morphologies: (a) AM60_HTlc^{30 min} (b) AM60^{0.02}_HTlc^{30 min} and (c) AM60^{0.22}_HTlc^{30 min} (d) GAXRD patterns: AM60_HTlc, AM60^{0.02}_HTlc and AM60^{0.22}_HTlc treated for 30 min.

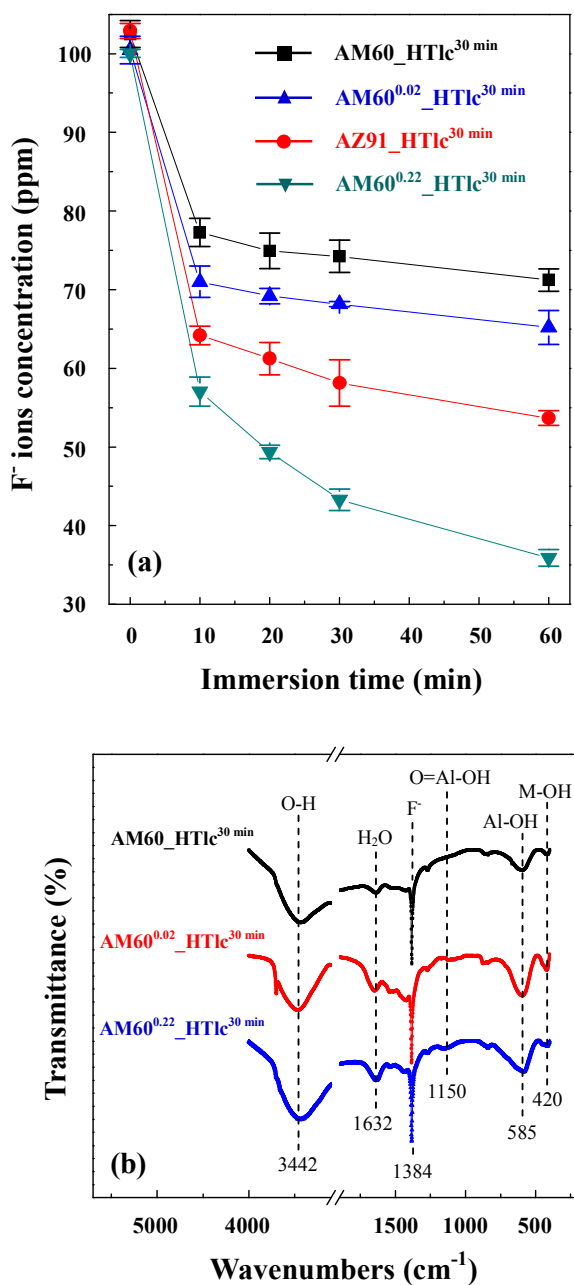


Fig. 13 (a) Remove amount of fluoride ions (ppm) versus immersion time in a fluoride aqueous solution (100 ppm) at pH 6 by 1.5 g AM60_HTLc^{30 min}, AZ91_HTLc^{30 min}, AM60^{0.02}_HTLc^{30 min} and AM60^{0.22}_HTLc^{30 min}: (b) the samples' IR spectra after 60 min of F⁻ uptaking experiments.

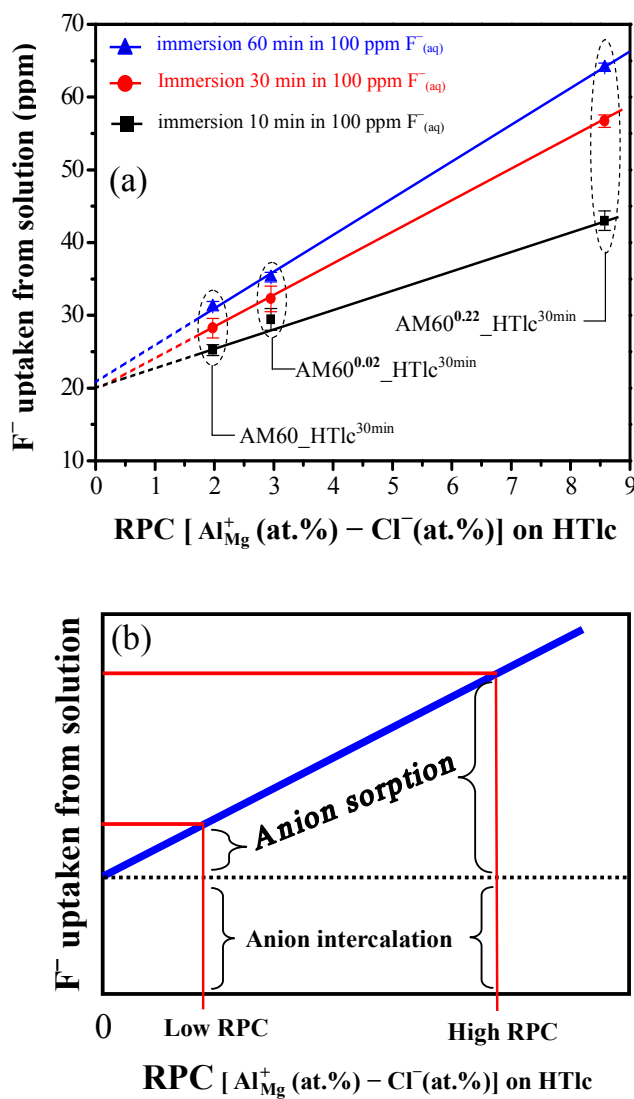


Fig. 14 (a) F^- uptaken from solution (ppm) vs. RPC $[Al_{Mg}^+ (at\%) - Cl^- (at\%)]$. Herein, RPC means residual positive charges; (b) a schematic plot showing that the mechanism of anion sorption became dominant as the RPC of the HTlc increased.